ACS APPLIED MATERIALS & INTERFACES

Research Article

www.acsami.org

Co_3O_4-Modified TiO_2 Nanotube Arrays via Atomic Layer Deposition for Improved Visible-Light Photoelectrochemical Performance

Bin Huang,[†,‡] Wenjuan Yang,[‡] Yanwei Wen,[‡] Bin Shan,*[,‡] and Rong Chen*[,†]

[†]State Key Laboratory of Digital Manufacturing Equipment and Technology, School of Mechanical Science and Engineering and [‡]State Key Laboratory of Materials Processing and Die and Mold Technology, School of Materials Science and Engineering, Huazhong University of Science and Technology, Wuhan 430074, Hubei, People's Republic of China

Supporting Information

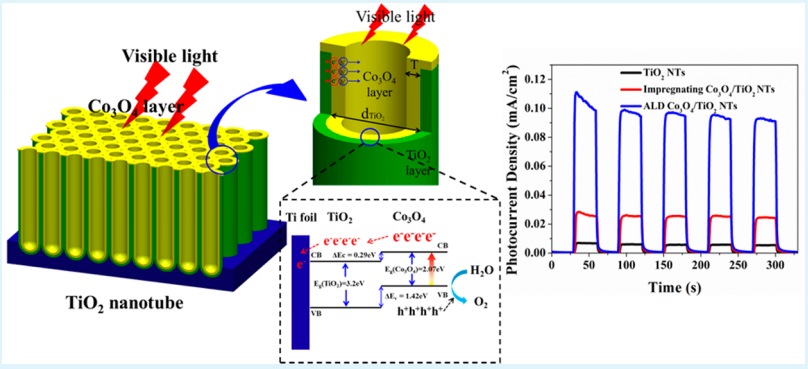

ABSTRACT: Composite Co_3O_4/TiO_2 nanotube arrays (NTs) were fabricated via atomic layer deposition (ALD) of Co_3O_4 thin film onto well-aligned anodized TiO_2 NTs. The microscopic morphology, composition, and interfacial plane of the composite structure were characterized by scanning electron microscopy, energy dispersion mapping, X-ray photoelectron spectra, and high-resolution transmission electron microscopy. It was shown that the ultrathin Co_3O_4 film uniformly coat onto the inner wall of the high aspect ratio (>100:1) TiO_2 NTs with film thickness precisely controlled by the number of ALD deposition cycles. The composite structure with ~4 nm Co_3O_4 coating revealed optimal photoelectrochemical (PEC) performance in the visible-light range (λ > 420 nm). The photocurrent density reaches as high as 90.4 $\mu A/cm^2$, which is ~14 times that of the pristine TiO_2 NTs and 3 times that of the impregnation method. The enhanced PEC performance could be attributed to the finely controlled Co_3O_4 coating layer that enhances the visible-light absorption, maintains large specific surface area to the electrolyte interface, and facilitates the charge transfer.

KEYWORDS: *titanium oxide, heterostructure, atomic layer deposition, cobalt oxide, photoelectrochemical, visible light*

INTRODUCTION

Over the past decades, nanoscale TiO_2 has been widely investigated for photocatalysis and dye-sensitized solar cell applications due to its low cost, nontoxic, photostable properties, and strong photooxidation ability.[1−8] Recently, highly ordered TiO_2 nanotube arrays (NTs) fabricated by anodization method have attracted much attention for their outstanding chemical and mechanical stability, large specific area, and good charge-transfer properties.[9−12] However, the intrinsic band gap of TiO_2 (3.2 eV for anatase and 3.0 eV for rutile) limits its optical absorption to the UV region, which only accounts for less than 4% of the total solar radiation.[13−15] Different approaches have been explored to improve the photoelectrochemical (PEC) activities of TiO_2 in the visible-light region, including metal/nonmetal doping, dye sensitization, and heterojunction formation.[16−25]

Coupling TiO_2 NTs with a narrow band gap semiconductor is a promising approach to enhance the visible-light absorption, as the photoexcited electrons and holes from the narrow gap semiconductor, if separated effectively, could significantly promote the visible-light PEC performance.[12,15,26−29] Co_3O_4, a typical p-type transition metal oxide with a band gap of ~2.07 eV,[30] has been proposed as a candidate material coupling with TiO_2 nanostructure for its abundance and unique optical and catalytic properties.[31−36] To date, several wet synthesis methods have been employed to fabricate Co_3O_4/TiO_2 composite nanostructures. Wang et al. reported the Co_3O_4/TiO_2 hierarchical structure synthesized by hydrothermal method exhibited improved charge-transfer ability.[37] Wang et al. reported that the nanocomposite of powdered $CoOx/TiO_2$ exhibited high photoactivity of hydrogen generation.[38] Cao et al. described the fabrication of heterostructure of Co_3O_4/TiO_2 nanorod arrays by a two-step solution-based method.[39] The photocurrent density of Co_3O_4 nanoparticles modified TiO_2

Received: September 18, 2014
Accepted: December 10, 2014
Published: December 10, 2014

Scheme 1. Synthesis Process of ALD Cobalt Oxide Modified TiO_2 NTs

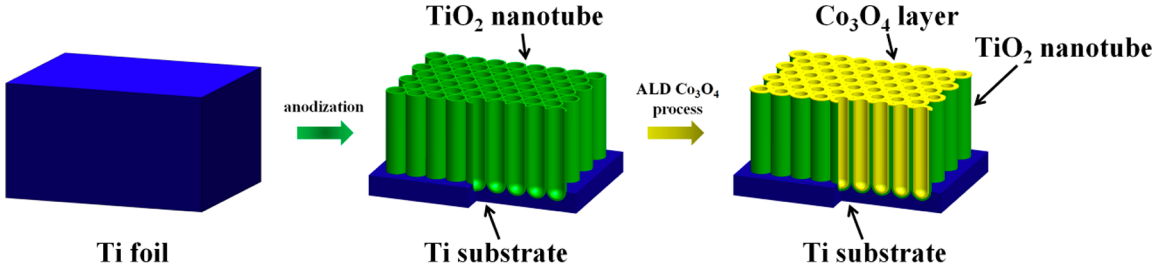

nanorod fabricated could reach up to 40 $\mu A/cm^2$ under visible-light illumination.[39] However, achieving precise control of the coating morphology still remains a great challenge. For example, electrolyte-based cathodic deposition of cobalt oxide onto TiO_2 NTs tends to produce large oxide particles clogging the nanotube structure that hinders the further promotion of PEC activities.[40]

To achieve better coating uniformity, atomic layer deposition (ALD) technique has been recently utilized for the growth of conformal layers onto three-dimensional nanostructures.[41−43] For example, Luo et al. reported the highly controllable and homogeneous coating of ZnO on arbitrary TiO_2 substrate by ALD for improved photoconversion efficiency.[41] Hwang et al. demonstrate that the epitaxial of rutile TiO_2 shell on TiO_2 nanowires by ALD can enhance the charge-collection ability.[19] However, uniform coating of ALD Co_3O_4 on high aspect ratio TiO_2 NTs has not been reported to our best knowledge, and the optimal Co_3O_4 thickness on TiO_2 tubes for PEC performance remains unclear. It is therefore much desirable to develop a reliable ALD process of coating TiO_2 NTs with good uniformity and investigate the charge-transfer mechanism for PEC applications.

We report here the successful fabrication of Co_3O_4/TiO_2 NTs composite with well-controlled thickness using ALD. Our ultrathin Co_3O_4 film coated by ALD uniformly extends throughout the whole TiO_2 NT channels with aspect ratios over 100:1, as verified by scanning electron microscopy (SEM) and energy dispersion mapping (EDX). X-ray photoelectron spectroscopy (XPS), X-ray diffraction (XRD), Raman spectroscopy, and high resolution transmission electron microscopy (HR-TEM) further confirm the formation of Co_3O_4/TiO_2 heterojunction. The band offsets of the heterojunctions Co_3O_4/TiO_2 is measured using high-energy resolution core-level and valence-band XPS. The thickness of Co_3O_4 layer can be finely controlled by the number of ALD cycles with the optimal PEC performance obtained at a Co_3O_4 layer thickness of ∼4 nm. The conformal coating not only provides improved visible light absorption but also forms the hetorojunction to enhance the separation of the photogenerated electron−hole pairs. With good stability and low contact resistance at the interface, the ALD-fabricated Co_3O_4/TiO_2 NTs show superior PEC performance under visible light illumination and could achieve photocurrent density as high as 90.4 $\mu A/cm^2$, which is about three times higher than impregnation-synthesized heterojunctions and 1 order of magnitude higher than that of pristine TiO_2 NTs. Our analyses show that the enhanced PEC performance could be attributed to the improved charge-transfer ability due to thin-film coating by ALD. The technique could be readily transferred to the coating of other high-aspect ratio nanotube or nanoporous materials.

EXPERIMENTAL SECTION

Preparation of ALD Co_3O_4/ TiO_2 NTs. Ti foils (>99.5%) with 0.5 mm thickness were first degreased ultrasonically in acetone, ethanol, and deionized water sequentially for 10 min. Then the self-organized TiO_2 NTs was prepared via a two-step anodization method with platinum slice as anode electrode. An ethylene glycol solution containing 0.25 wt % NH_4F and 2 wt % H_2O was used as electrolyte with 60 V anodic potential provided by a direct current power. The duration of first step anodization was set to 9 h. After that the as-grown membrane was removed by ultrasonication in deionized water. Then the second step anodization was conducted at the same condition for 1 h. Subsequently the samples were rinsed with ethanol and dried in oven at 100 °C for 30 min. Finally the obtained TiO_2 NTs were annealed at 500 °C in air for 3 h with a ramping rate of 2 °C/min to form anatase phase.

ALD cobalt oxide was grown in a commercial ALD system SUNALE R200 reactor. Bis(cyclopentadienyl)cobalt(II) ($Co(Cp)_2$, 98%, Strem Chemicals) and O_3 (∼11% in volume) were used as precursors. High-purity nitrogen (99.999%) was used as the sources carrier and purging gas. The cobaltocene was heated to 100 °C, and the deposition temperature was maintained at 150 °C to obtain smooth cobalt oxide film. The cobalt oxide thickness was controlled by adjusting the number of ALD cycles. The whole synthesis process of ALD Co_3O_4/TiO_2 NTs is illustrated in Scheme 1. The obtained highly ordered titanium oxide nanotube was used as substrate for the deposition of cobalt oxide with different ALD cycles. After ALD deposition, samples were annealed at 200 °C for 5 h.

For comparison, the impregnating method was also used to deposit cobalt oxide onto TiO_2 NTs. The annealed TiO_2 NTs was immersed into 0.3 M $Co(NO_3)_2$ solution, distilled water, 0.3 M Na(OH) solution, and distilled water alternatively for 30 min. Such cycle was repeated several times followed by annealing in a tube furnace at 200 °C for 5h.

Characterization. The morphology and composition of Co_3O_4/TiO_2 NTs samples was characterized by field scanning electron microscope (JEOL-6200, Japan) and energy dispersion mapping (X-Max Oxford Instrument). Raman spectroscopy (LabRAM HR800) was conducted to determine the nanocomposite structure with 532 nm laser excitation. The crystalline phase of samples was identified by X-ray diffraction using an Analytical X'Pert Pro diffractometer with Cu Kα radiation (λ = 0.154 18 nm). UV−vis diffuse reflectance spectra (UV-DRS) were obtained on a Lambda 750S (PerkinElmer) spectrometer using $BaSO_4$ as the reference. The chemical composition was analyzed by X-ray photoelectron spectroscopy (VG Multilab 2000) using a monochromatic Al Kα X-ray radiation. The band alignment of Co_3O_4/TiO_2 was determined by measuring the core-level and valence-band (VB) spectra. Data were fitted with XPSPEAK4.1 software, and binding energy was calibrated with respect of C 1s (284.6 eV). The composition, microstructure, and the presence of p−n junction was further examined by HR TEM (JEOL-2010FEF) operated at an acceleration voltage of 200 kV.

The PEC performance of as-prepared samples was measured in a three-electrode system containing Pt foil as the counter electrode, a saturated calomel electrode (SCE) as reference electrode, and samples as working electrode. 0.1 M Na_2SO_4 solution was used as electrolyte. A 500W Xe lamp equipped with an ultraviolet cutoff filter (λ > 420 nm)

dx.doi.org/10.1021/am506392y | ACS Appl. Mater. Interfaces 2015, 7, 422−431

was utilized to simulate the visible-light source. The samples with 1 cm^2 active area were illuminated with light intensity of 100 mW/cm^2 calibrated by a radiometer. All electrochemical experiments were conducted under ambient condition. The data were recorded through an electrochemical workstation (Autolab, PGSTAT 302N). The photoconversion efficiency (η) was plotted as a function of applied potential, using the following formula:

$$\eta(\%) = \frac{[(\text{total power output} - \text{electrical power input})]}{[\text{light power input}]} \times 100$$

$$= j_p[E^0_{rev} - |E_{app}|] \times 100/I_0$$

where j_p is the photocurrent density (mA/cm^2), $j_pE^0_{rev}$ is the total power output, $j_p|E_{app}|$ is the electrical power input, I_0 is the power density of the incident light (mW/cm^2), E^0_{rev} is the standard reversible potential, which is 1.23 V versus NHE, and the applied potential $E_{app} = E_{meas} - E_{aoc}$, where E_{meas} is the electrode potential (vs SCE) of the working electrode at which the photocurrent was measured under illumination and E_{aoc} is the electrode potential (vs SCE) of the same electrode at an open circuit under the same condition.

RESULTS AND DISCUSSION

Characterization of the Composite Co_3O_4/TiO_2 NTs. Figure 1 displays the FE-SEM images of the tube diameter

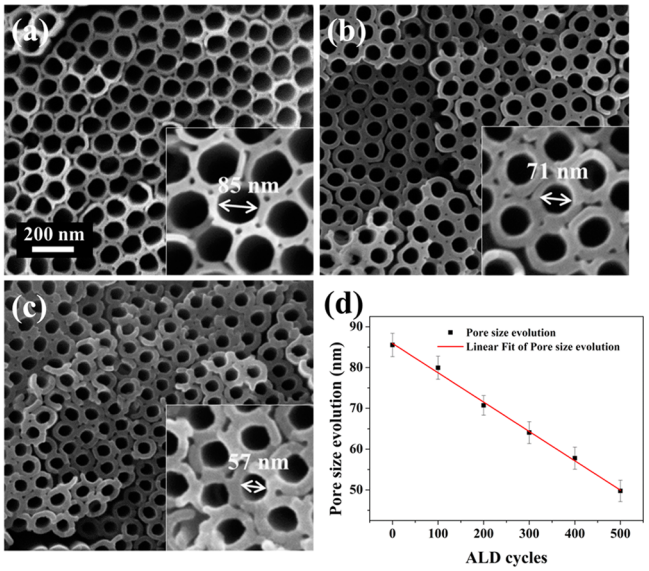

Figure 1. SEM images of (a) pure TiO_2 NTs and after (b) 200 and (c) 400 cycles of ALD cobalt oxide deposition. (d) Pore size evolution as a function of ALD cycles.

evolution before and after cobalt oxide coating by ALD technique. The structure of pristine TiO_2 NTs is highly ordered and well-aligned on Ti foil with smooth surface and an average tube inner diameter of 85 nm (Figure 1a). The pore size decreases linearly with the ALD cobalt oxide deposition cycles, from ~70 (Figure 1b) to ~57 nm (Figure 1c) with the number of ALD cycles increased from 200 to 400 cycles. In all cases the nanotubular structures are preserved well without blocking of the nanochannels or forming large particles, which would facilitate the charge transportation through the interface between the electrolyte and the tube inner wall. From the slope of the linear curve correlating pore size with the ALD cycles (Figure 1d), the growth rate of cobalt oxide on TiO_2 NTs is estimated to be ~0.4 nm/cycle, which is consistent with the growth rate of Co_3O_4 on reference Si wafer (Supporting Information, Figure S1). As a comparison, the morphology of Co_3O_4/TiO_2 NTs samples prepared by impregnating method was also analyzed. It could be seen that part of the TiO_2 NTs surface is blocked by the large cobalt oxide particles (Supporting Information, Figure S2). The hierarchical structure of the TiO_2 NTs scaffold and the uniformly ALD-coated Co_3O_4 film may allude to the interfacial interaction, which will be discussed in later paragraphs.

EDX elemental mapping analysis was conducted on the cross section of Co_3O_4/TiO_2 NTs by ALD to evaluate the coating conformity of cobalt oxide throughout the channels of TiO_2 NTs. The results presented in Figure 2 clearly reveal the

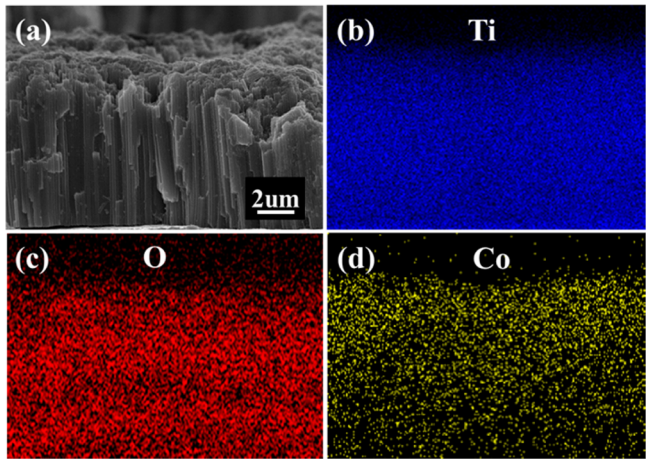

Figure 2. (a) Cross-sectional SEM image of Co_3O_4/TiO_2 NTs and EDX elemental mapping image to the corresponding area: (b) Ti, (c) O, and (d) Co.

presence of cobalt oxide throughout the whole channels. The dispersion of cobalt in Figure 2d is similar to titanium and oxygen in Figure 2b,c with satisfying uniformity. Note that the length of the nanotube was approximately 10 μm, giving an aspect ratio of ~110:1. The result demonstrates the capability of ALD technology in coating nanotube channels with well-controlled film thickness and coating uniformity.

To reveal the composition of the samples, XPS study was conducted on the Co_3O_4/TiO_2 NTs composite fabricated by ALD to probe the chemical composition and elemental valence. The spectra survey illustrated in Figure 3a demonstrates the existence of Co, Ti, O, and adventitious C. Fine scan XPS spectrum of Ti is shown in Figure 3b, with two peaks of Ti 2p observed at binding energies of ~459.2 and ~464.8 eV, respectively. These peaks can be assigned to Ti $2p_{3/2}$ and Ti $2p_{1/2}$, consistent with the XPS data of Ti^{4+} in anatase phase.[15] The XPS analysis indicates the coating of Co_3O_4 by ALD does not affect the elemental properties of the TiO_2 substrate. As for Co peaks, the binding energies located at ~780.4 and ~796.1 eV can be assigned to Co $2p_{3/2}$ and Co $2p_{1/2}$ (Figure 3c).[44−46] In addition, the main peaks are accompanied by weak shake up satellites located at 8.0 eV higher binding energy side. Such peaks are typical signatures of Co_3O_4 and consistent with literatures.[31,44,45] The fitting result of O 1s is shown in Figure 3d. The peak located at ~532.0 eV was designated to adsorbed oxygen on the surface. The other two peaks were attributed to the O in TiO_2 (~530.2 eV) and Co_3O_4 (~530.9 eV), respectively. Raman and XRD were both employed on thicker samples. The Raman result shows the typical vibration modes of anatase and Co_3O_4 by ALD and impregnation samples

dx.doi.org/10.1021/am506392y | ACS Appl. Mater. Interfaces 2015, 7, 422−431

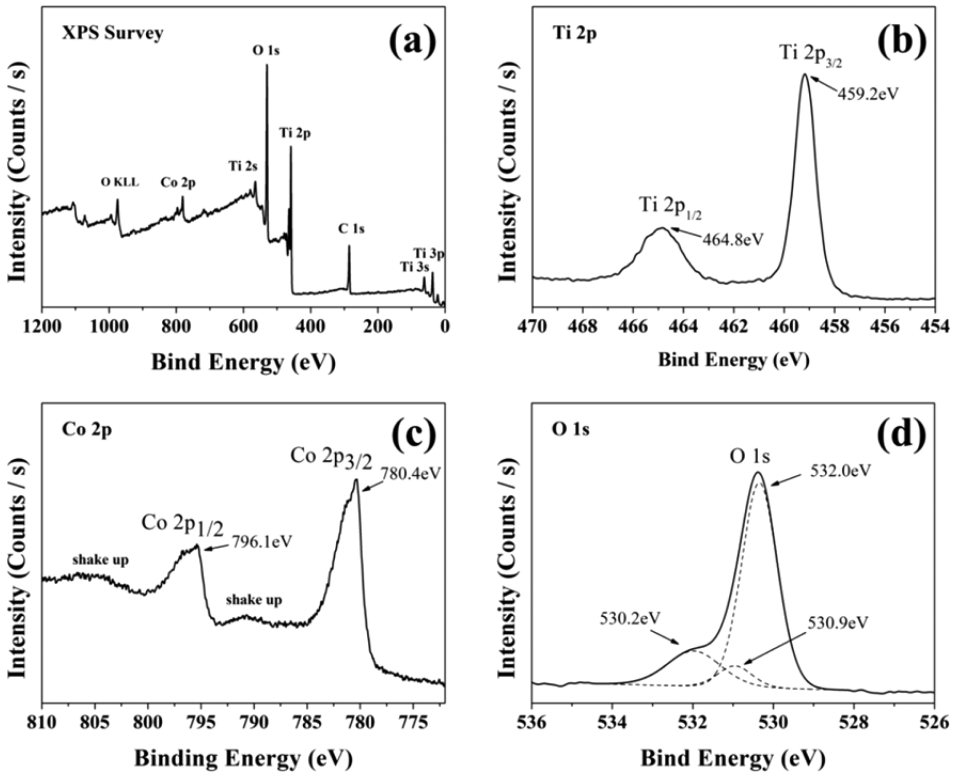

Figure 3. (a) Co_3O_4/TiO_2 NTs XPS spectra survey and (b) Ti 2p spectra, (c) Co 2p spectra, and (d) O 1s spectra.

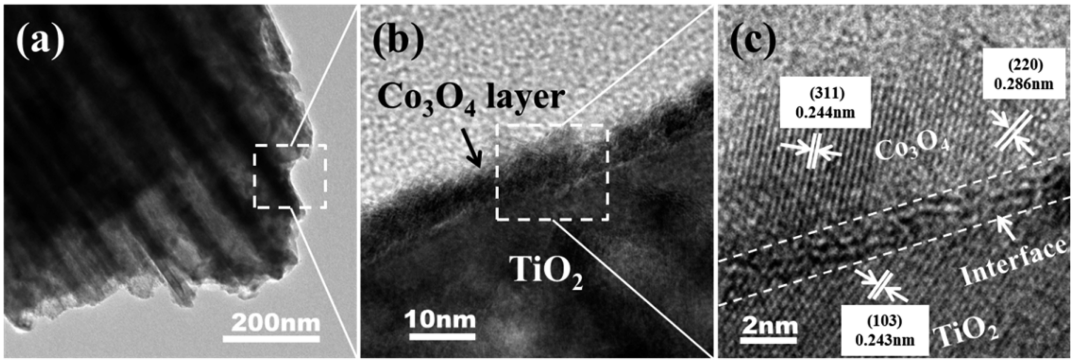

Figure 4. (a) TEM image of ALD Co_3O_4/TiO_2 NTs and (b) zoomed area of the heterostructure Co_3O_4/TiO_2 NTs. (c) High-resolution TEM image of Co_3O_4/TiO_2 interface.

(Supporting Information, Figure S3).[47] The XRD patterns further confirm the formation of anatase TiO_2 and spinel Co_3O_4 (Supporting Information, Figure S4). The XPS, Raman, and XRD measurements verify the formation of Co_3O_4/TiO_2 composite structure without introducing other impurity phases.

The interface and the crystalline structure of the obtained Co_3O_4/TiO_2 NTs were characterized by TEM as shown in Figure 4. There is no agglomerated particle formation on the TiO_2 surface (Figure 4a), which is consistent with the SEM observations. Figure 4b shows the zoomed image of the square area in Figure 4a, where the heterostructure of Co_3O_4/TiO_2 is observed. The HR-TEM (Figure 4c) clearly reveals that both Co_3O_4 and TiO_2 are crystalline. The lattice fringes with the *d*-spacing of 0.286 and 0.244 nm can be assigned to (220) and (311) planes of Co_3O_4, and lattice fringes of 0.243 nm can be assigned to (103) plane in anatase TiO_2, respectively. The distinct boundary is a direct evidence for the formation of Co_3O_4/TiO_2 heterojunction.

Photoelectrochemical Performance. The optical properties of the Co_3O_4/TiO_2 NTs by ALD sample were studied by UV−vis diffuse reflectance spectroscopy with the result plotted in Figure 5. The adsorption onset of pure TiO_2 NTs begins at ∼390 nm, which is consistent with the band gap of bulk anatase (E_g = 3.2 eV, corresponding to λ = 387 nm). The broad absorption peak in the visible light region can be assigned to the scattering effect caused by pores or cracks in the nanotube arrays.[26] In contrast, the Co_3O_4/TiO_2 NTs shows significant enhancement in the visible light absorption range from 420 to 600 nm, due to the intrinsic narrow band gap of Co_3O_4 which could promote the visible light absorption ability. As expected, the light absorption of the Co_3O_4/TiO_2 NTs samples by ALD is effectively extended into the visible range compared with that of pure TiO_2 NTs.

The photocurrent measurements were conducted to investigate the PEC properties of the pristine TiO_2 NTs and Co_3O_4/TiO_2 NTs. All measurements were carried out in 0.1 M

dx.doi.org/10.1021/am506392y | ACS Appl. Mater. Interfaces 2015, 7, 422−431

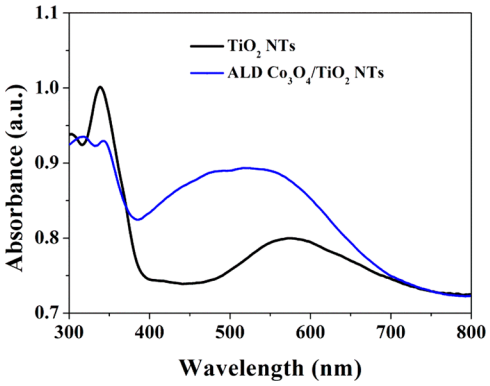

Figure 5. UV−vis diffuse reflectance spectra of TiO_2 NTs and ALD Co_3O_4/TiO_2 NTs sample.

Na_2SO_4 solution under visible light illumination (λ > 420 nm). The PEC performance for the samples prepared by impregnation method was also presented with the optimal photocurrent after five cycles (Supporting Information, Figure S4). Linear sweep voltammograms measurement of pure TiO_2 NTs, impregnation method prepared Co_3O_4/TiO_2 NTs and ∼4 nm coated Co_3O_4/TiO_2 NTs by ALD are shown in Figure 6a. Both ALD and impregnation method prepared Co_3O_4/TiO_2 NTs show an enhancement of photocurrent density compared to that of the pure TiO_2 throughout the whole potential region, indicating the promotion of the visible light harvesting ability after Co_3O_4 modification. The saturated photocurrent density of ALD Co_3O_4/TiO_2 NTs electrode (90.4 $\mu A/cm^2$) is approximately 14 times that of pristine TiO_2 NTs (6.5 $\mu A/cm^2$) and 3 times higher than that by the impregnation prepared Co_3O_4/TiO_2 NTs (29.2 $\mu A/cm^2$). The corresponding photoconversion efficiency as a function of applied potential is shown in Figure 6b. The E_{aoc} was determined to be −0.237, −0.258, and −0.287 V versus saturated calomel electrode (SCE) for pure TiO_2 NTs, impregnation method prepared Co_3O_4/TiO_2 NTs and ALD method prepared Co_3O_4/TiO_2 NTs, respectively (Figure 6a). The power density (I_0) of the incident light was 100 mW/cm^2 in the experimental condition. Taking these data into the equation we obtain that the maximum photoconversion efficiency of 0.084% for ALD Co_3O_4 modified TiO_2 NTs is observed at a voltage bias of −0.129 V versus SCEunder visible light irradiation, while the pure TiO_2 NTs shows only 0.0146% at the bias of −0.131 V and the impregnation system shows 0.0196% at the bias of 0.182.[47] The different PEC performance of samples by these two methods indicates that the detailed morphology control of Co_3O_4 layer on TiO_2 NTs plays an important role in the PEC process. The pure TiO_2 NTs and Co_3O_4/TiO_2 NTs photoelectrodes were further tested under intermittent illumination of visible light with a bias of 0.2 V versus SCE. As shown in Figure 6c, all electrodes show quick photo response that the photocurrent increases immediately after light illumination and decays to the origin value once the illumination is switched off. Compared to pure TiO_2 NTs, the photocurrent density for ALD fabricated Co_3O_4/TiO_2 NTs shows more than 1-fold increase.

Mechanism Discussion. To explore the mechanism of the enhanced PEC performance of the Co_3O_4/TiO_2 NTs, electrochemical impedance spectroscopy (EIS) was chosen to probe the electro-hole separation and transfer with frequencies ranging from 100 kHz to 0.01 Hz. The results presented in

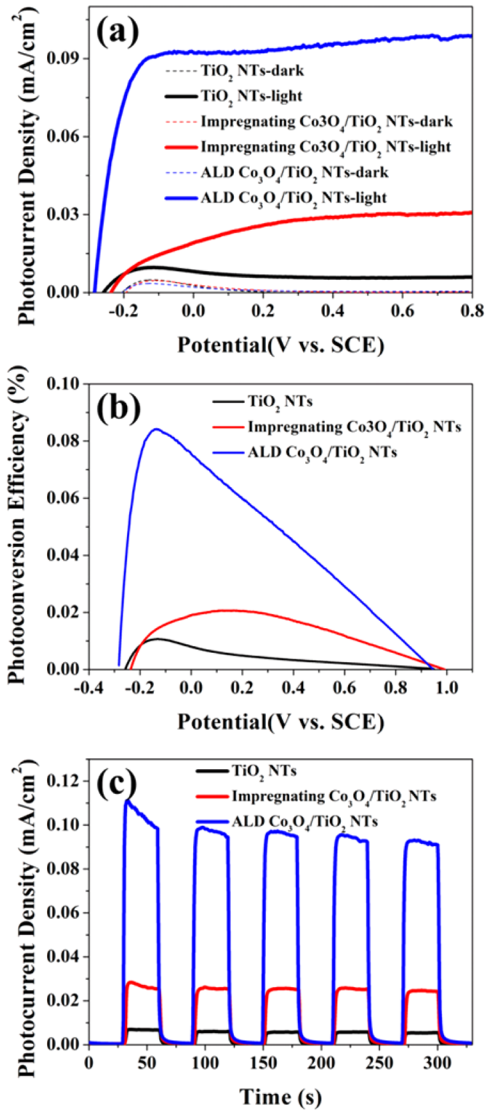

Figure 6. (a) Current density vs bias potential curves (vs SCE). (b) Photoconversion efficiency. (c) Photocurrent density vs time of pristine TiO_2 NTs, impregnation method prepared Co_3O_4/TiO_2 NTs and 100 ALD cycles Co_3O_4/TiO_2 NTs. Test condition: 100 mW/cm^2 visible light illumination (λ > 420 nm) in 0.1 M Na_2SO_4 solution.

Figure 7 show the Nyquist curve of pure TiO_2 NTs, impregnation samples, and ∼4 nm ALD Co_3O_4/TiO_2 NTs measured in 0.1 M Na_2SO_4 solution in dark condition and under visible-light illumination, respectively. All Nyquist plots (Figure 7a,b) display a hemisphere at high frequencies whose diameter represents the electron-transfer resistance controlling the kinetics at the electrode surface. The straight line occurred at low frequency is related to the diffusion process. The corresponding equivalent circuit is depicted in the inset of Figure 7, where R_s stands for bulk resistance, originating from the electrolyte and electrode, R_{ct} is the charge-transfer resistance, C_{dl} is the double-layer capacitance, and W stands for the Warburg impedance originated from the diffusion process at the electrode surface. Evidently, the charge-transfer resistance in dark condition is larger than visible-light illumination for all samples. The Co_3O_4/TiO_2 NTs by ALD reveals the smallest R_{ct} under light illumination conditions.

The fitting result of charge transfer resistance and the corresponding photocurrent density under short-circuit is listed

dx.doi.org/10.1021/am506392y | ACS Appl. Mater. Interfaces 2015, 7, 422−431

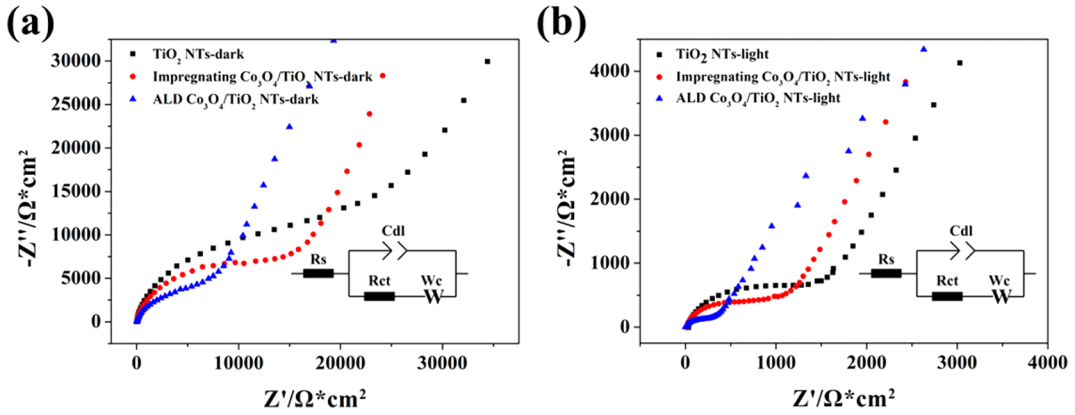

Figure 7. EIS Nyquist plots for TiO_2 NTs and Co_3O_4/TiO_2 NTs under (a) dark condition and (b) visible-light illumination.

in Table 1. After deposition of Co_3O_4 onto the TiO_2 NTs, the value of R_{ct} decreases, indicating easier charge transfer across the interface. Compared with pure TiO_2 NTs and electrolyte method fabricated Co_3O_4/TiO_2 NTs composite, the ALD photoelectrode shows considerably smaller charge transfer resistance of ~543.8 Ωcm^2. The result is consistent with the highest photocurrent density of that the ALD Co_3O_4/TiO_2 NTs. The EIS measurement gives strong evidence that the conformal coating of Co_3O_4 onto TiO_2 NTs by ALD can greatly improve the charge transfer properties and display efficient separation of photoexcited electron−hole pair.

Table 1. EIS Fitting Parameters of TiO_2 NTs and Co_3O_4/TiO_2 NTs Samples and the Corresponding Photocurrent Density under Visible Light Illumination Condition

samples	R_{ct} ($\Omega \times cm^2$)	photocurrent density ($\mu A/cm^2$)
TiO_2 NTs (light)	1437.2	6.5
impregnating-Co_3O_4/TiO_2 NTs (light)	986.7	29.2
ALD-Co_3O_4/TiO_2 NTs (light)	543.8	90.4

The EIS result reveals that the structure of conformal coating of Co_3O_4 thin film layer is more suitable for the carriers transfer compared to the Co_3O_4 particles onto TiO_2 NTs. Since the oxide thickness is thought to be a crucial factor leading to the recombination of photogenerated electron−hole pairs,[41] it is interesting to study the effect of Co_3O_4 layer thickness on PEC performance. The photocurrent density measurements for a number of samples with different ALD coated thickness are shown in Figure 8a. It can be observed that the photocurrent density of Co_3O_4/TiO_2 NTs increases with the Co_3O_4 layer thickness initially and reaches a maximum point at the thickness of 4 nm, beyond which the photocurrent density would decrease. This implies that there is an optimal coating thickness of Co_3O_4 in promoting the PEC performance of the TiO_2 NTs. In general, the photocurrent density is correlated to both the number of photoexcited carriers and surface reaction rate on the electrode. In our experiment, the initial tube structure has a diameter of d_{TiO_2} (~85 nm) as shown in Figure 1a. Its diameter would decrease with varying Co_3O_4 coating thickness of T (as a function of ALD cycles). When illuminated under visible light (Figure 8b), the electrons and holes can be excited within the Co_3O_4 layer that would be proportional to the light intensity (by a factor β). After the process of photoexcitation, the electrons will diffuse to the TiO_2 nanotubes, through which

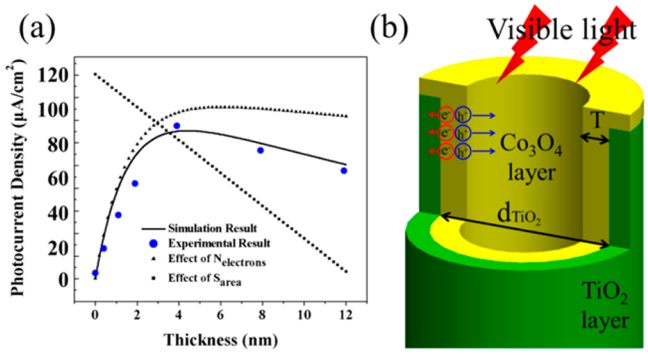

Figure 8. (a) Evolution of photocurrent density and simulation result as a function of Co_3O_4 thickness. (b) Schematic picture of the tube structure of TiO_2/Co_3O_4 composite with a coating thickness of T.

they will be conducted to the outer circuit. The total number of photoexcited electrons ($N_{electrons}$) reaching the TiO_2 nanotube surface thus can be approximated by integrating over the Co_3O_4 thickness (T):

$$N_{electrons} = \int_0^T \beta \times I_0 e^{-\alpha x} \times e^{-(T-x)/L_n} dx$$

where I_0 is the light intensity at the materials interface at $x = 0$, α is the absorption coefficient, L_n is the diffusion length of Co_3O_4, and $(T - x)$ is the length that the electron must go across before reaching the TiO_2 surface. It was reported that α varies from ~0.01 nm^{-1} to 0.03 nm^{-1} with the wavelength changing from 400 to 1200 nm.[48] Since the value of α has little effect on the overall conversion, we approximate it by a value of 0.01 nm^{-1}.

Besides the diffusion process of electrons, there will also be a limitation of the surface area on the oxidation reaction of photoanode. For the NTs, the tube diameter decreases linearly with the thickness of the Co_3O_4 layer (as given by $d_{TiO_2} - 2 \times T$). Accordingly, combining the effect of charge transfer and surface area, finally we get the following formula:

$$\text{photocurrent}_{simulation} = \mu \times N_{electrons} \times S_{area}$$

$$= \mu \times \int_0^T \beta \times I_0 e^{-\alpha x} \times e^{-(T-x)/L_n} dx \times \frac{d_{TiO_2} - 2 \times T}{d_{TiO_2}}$$

where the factor μ stands for the conversion coefficient, and S_{area} stands for the function of surface area. The fitting result is illustrated in Figure 8a. The simulation result reveals a relatively

dx.doi.org/10.1021/am506392y | ACS Appl. Mater. Interfaces 2015, 7, 422−431

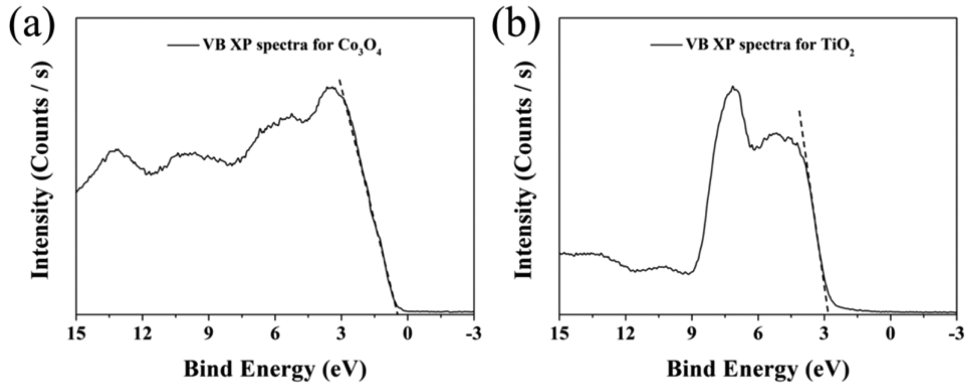

Figure 9. Valence band XPS for (a) Co_3O_4 and (b) TiO_2.

short minority diffusion length of ALD fabricated Co_3O_4 (~2 nm), similar to that of hematite.[49] The evolution tendency of $N_{electrons}$ and S_{area} as a function of Co_3O_4 layer thickness are also plotted (dash line in Figure 8a). It can be seen that when the thickness is relatively small, the number of electrons increases with the increase of thickness. However, further increase of the layer thickness forms relatively thick oxide layer, which causes increased carrier recombination rate,[41,50] and reduced the inner diameter of the nanotubes and the contact area with the electrolyte. Hence, these two competing factors result in an optimal Co_3O_4 thickness of ~4 nm. This conclusion is also consistent with the EIS results. For Co_3O_4/TiO_2 NTs by impregnation method, the Co_3O_4 particles (with the size >100 nm) aggregate on the surface of TiO_2 NTs that are larger than the diffusion length. Therefore, the charge carriers are hard to effectively transfer through the Co_3O_4 particles due to the severe recombination. Besides, the blocked tube structure by Co_3O_4 particles provides little effective contact area, which hinders the PEC reaction. In contrast, the structure of uniform coating Co_3O_4 layer by ALD is desirable to balance the recombination and preserve the large surface area. Thus, a relatively higher PEC performance is obtained with the highest photocurrent density under visible-light illumination much higher than recently reported Co_3O_4/TiO_2 nanorod system prepared via wet chemical approaches under similar measurement conditions.[39]

The band alignment of the composite structure is crucial to further understand the enhanced photoactivity of the Co_3O_4/TiO_2 heterostructure. Here the XPS of core-level and valence band spectra were conducted to calculate the band offsets. The valence band maxima (VBM) for the individual materials were determined by band XPS (Figure 9) with a liner extrapolation method. VBM was found to be 0.56 and 2.78 eV for Co_3O_4 and TiO_2, respectively. The binding energy difference was checked by core-level XPS (Supporting Information, Figure S6). After combination, the binding energy changed from 459.41 to 459.22 eV for Ti $2p_{3/2}$ and from 779.82 to 780.43 eV for Co $2p_{3/2}$.

With the core-level positions and VBM of the heterojunctions values,[51] the valence band offset (VBO) can be calculated by the following equation (data were summarized in Table 2):

$$\Delta E_V(Co_3O_4/TiO_2) = (E_{Co2p} - E_{VBM})_{Co_3O_4} - (E_{Ti2p} - E_{VBM})_{TiO_2} - (E_{Co2p} - E_{Ti2p})_{Co_3O_4/TiO_2}$$

Table 2. VBM and Core-Level Binding Energies of TiO_2 NTs and Co_3O_4/TiO_2 NTs Samples

materials	Co_3O_4	TiO_2	Co_3O_4/TiO_2
Co $2p_{3/2}$ (eV)	779.82		780.43
Ti $2p_{3/2}$ (eV)		459.41	459.22
VBM (eV)	0.56	2.78	

Here, $(E_{Co\ 2p} - E_{VBM})_{Co_3O_4}$ is the energy difference between Co 2p and VBM in the pure Co_3O_4 film. $(E_{Ti\ 2p} - E_{VBM})_{TiO_2}$ is the energy difference between Ti 2p and VBM in the TiO_2 nanostructure. $(E_{Co\ 2p} - E_{Ti\ 2p})_{Co_3O_4/TiO_2}$ is the energy difference between the Ti 2p and Co 2p core levels in the Co_3O_4/TiO_2 heterostructures. Hence, the measured valence-band offset is found to be 1.42 eV. Taking the band gaps for Co_3O_4 and TiO_2 to be 2.07 and 3.2 eV,[13,30] the value for conduction band offsets ΔE_C is found to be 0.29 eV.

The overall charge-transfer mechanism is illustrated in Figure 10. The heterojunction constructed by p-Co_3O_4 and n-TiO_2 plays an important role in the charge generation and separation of photoinduced electron−hole pairs. When the Co_3O_4 layer contacts with TiO_2, the Co_3O_4 could be easily excited and produce electrons in the conduction band minimum (CBM) and holes in the valence band maximum (VBM). The holes in VBM of Co_3O_4 will be consumed for the oxidation of water. Meanwhile, the excited electrons in CBM of Co_3O_4 side transfer to the CBM of TiO_2 and finally reach the Pt electrode for hydrogen generation in the PEC cell device.[39] Because of the evenly covered and intimate binding of the Co_3O_4 layer onto TiO_2 NTs by ALD method, the electron−holes pairs can be transferred smoothly through the one-dimensional tube channels. In contrast, the impregnation method tends to form relatively large-sized Co_3O_4 particles on TiO_2 NTs and blocks tube structure. The undesired structure suffers limited charge-transfer pathway with the large cobalt oxide particles acting as the electrons and holes recombination centers; thus, a lower visible-light PEC activity is observed. The enhanced carrier transfer rate of ALD fabricated composite arrays is due to several factors: First, the formation of Co_3O_4/TiO_2 heterostructure promotes the electron−hole separation under visible-light illumination. Second, the atomic layer growth of Co_3O_4 film in the interface of TiO_2 NTs by ALD maintains the large specific area, open-mouth morphology of the nanotube and provides effective charge-transfer route through the one-dimensional structure. Third, the well-controlled cobalt oxide thickness by ALD effectively minimizes the inner recombination of photogenerated electrons and holes; thus, the charges

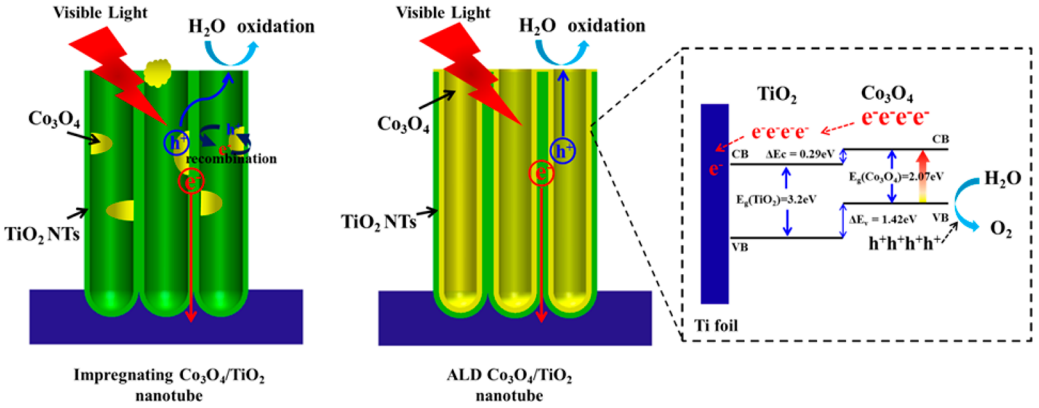

Figure 10. Schematic illustrating the charge separation and transfer under visible light for Co_3O_4/TiO_2 NTs fabricated by impregnating method and ALD method.

can be transferred more efficiently. Therefore, we conclude that the coating conformity and the large interfacial area are the main reasons for the superior visible-light PEC performance.

CONCLUSION

In summary, the Co_3O_4/TiO_2 NTs were fabricated by ALD method with excellent coating uniformity and accurately controlled thickness. The prepared ALD Co_3O_4/TiO_2 NTs structures show substantially improved visible-light PEC performance due to the enhanced visible-light absorbance and charge-transfer ability. The best performance was observed at ~4 nm ALD cobalt oxide coating. The maximum value of photocurrent reaches ~14 times that of pure TiO_2 NTs and 3 times that of impregnation-prepared Co_3O_4/TiO_2 NTs. This work demonstrates the utilization of ALD technology as a promising way of fabricating nanoscale composite structures for energy and environmental applications.

ASSOCIATED CONTENT

Supporting Information

The dependence of ALD cycles on thickness of Co_3O_4 on silicon wafer. SEM for impregnation method prepared Co_3O_4/TiO_2 NTs samples. Raman spectrum for pure TiO_2 and Co_3O_4/TiO_2 NTs samples. XRD diffraction patterns of ALD-prepared Co_3O_4/TiO_2 NTs samples. The intermittent photocurrent for impregnation method prepared Co_3O_4/TiO_2 NTs. The XPS binding energy difference for Co 2p and Ti 2p. This material is available free of charge via the Internet at http://pubs.acs.org.

AUTHOR INFORMATION

Corresponding Authors

*E-mail: rongchen@mail.hust.edu.cn. Phone: +86-27-87558744. Fax: +86-27-87558744. (R.C.)
*E-mail: bshan@mail.hust.edu.cn. (B.S.)

Notes

The authors declare no competing financial interest.

ACKNOWLEDGMENTS

The authors thank Q. Peng for insightful discussion. We also would like to acknowledge equipment supports from AMETEK lab and the technology support by the Analytic Testing Center of HUST. The authors thank Dr. Huang for the help of XPS characterization. This work is supported by the National Basic Research Program of China (2013CB934800), Natural Science Foundation of China (51101064), and the Fundamental Research Funds for the Central Universities, HUST (2014TS037). R.C. acknowledges the Thousand Young Talents Plan, the Recruitment Program of Global Experts, and Program for Changjiang Scholars and Innovative Research Team in University (No.: IRT13017). B.S. acknowledges the Hubei Province Funds for Distinguished Young Scientists (2014CFA018).

REFERENCES

(1) Zhang, Z. H.; Zhang, L. B.; Hedhili, M. N.; Zhang, H. N.; Wang, P. Plasmonic Gold Nanocrystals Coupled with Photonic Crystal Seamlessly on TiO_2 Nanotube Photoelectrodes for Efficient Visible Light Photoelectrochemical Water Splitting. *Nano Lett.* **2012**, *13*, 14−20.
(2) Grimes, C. A. Synthesis and Application of Highly Ordered Arrays of TiO_2 Nanotubes. *J. Mater. Chem.* **2007**, *17*, 1451−1457.
(3) Shin, Y.; Lee, S. Self-Organized Regular Arrays of Anodic TiO_2 Nanotubes. *Nano Lett.* **2008**, *8*, 3171−3173.
(4) Zhu, W.; Liu, X.; Liu, H. Q.; Tong, D. L.; Yang, J. Y.; Peng, J. Y. Coaxial Heterogeneous Structure of TiO_2 Nanotube Arrays with CdS as a Superthin Coating Synthesized *via* Modified Electrochemical Atomic Layer Deposition. *J. Am. Chem. Soc.* **2010**, *132*, 12619−12626.
(5) Feng, X. J.; Sloppy, J. D.; LaTempa, T. J.; Paulose, M.; Komarneni, S.; Bao, N. Z.; Grimes, C. A. Synthesis and Deposition of Ultrafine Pt Nanoparticles within High Aspect Ratio TiO_2 Nanotube Arrays: Application to the Photocatalytic Reduction of Carbon Dioxide. *J. Mater. Chem.* **2011**, *21*, 13429−13433.
(6) Zhang, J.; Bang, J. H.; Tang, C. C.; Kamat, P. V. Tailored TiO_2−$SrTiO_3$ Heterostructure Nanotube Arrays for Improved Photoelectrochemical Performance. *ACS Nano* **2009**, *4*, 387−395.
(7) Fan, J. D.; Fàbrega, C.; Zamani, R. R.; Hao, Y.; Parra, A.; Andreu, T.; Arbiol, J.; Boschloo, G.; Hagfeldt, A.; Morante, J. R.; Cabot, A. Enhanced Photovoltaic Performance of Nanowire Dye-Sensitized Solar Cells Based on Coaxial TiO_2@TiO Heterostructures with a Cobalt(II/III) Redox Electrolyte. *ACS Appl. Mater. Interfaces* **2013**, *5*, 9872−9877.
(8) Lee, W. J.; Lee, J. M.; Kochuveedu, S. T.; Han, T. H.; Jeong, H. Y.; Park, M.; Yun, J. M.; Kwon, J.; No, K.; Kim, D. H.; Kim, S. O. Biomineralized N-Doped CNT/TiO_2 Core/Shell Nanowires for Visible Light Photocatalysis. *ACS Nano* **2011**, *6*, 935−943.
(9) Tsui, L. k.; Homma, T.; Zangari, G. Photocurrent Conversion in Anodized TiO_2 Nanotube Arrays: Effect of the Water Content in Anodizing Solutions. *J. Phys. Chem. C* **2013**, *117*, 6979−6989.
(10) Reyes-Gil, K. R.; Robinson, D. B. WO_3-Enhanced TiO_2 Nanotube Photoanodes for Solar Water Splitting with Simultaneous Wastewater Treatment. *ACS Appl. Mater. Interfaces* **2013**, *5*, 12400−12410.

(11) Xiao, F. X. Construction of Highly Ordered ZnO−TiO_2 Nanotube Arrays (ZnO/TNTs) Heterostructure for Photocatalytic Application. *ACS Appl. Mater. Interfaces* **2012**, *4*, 7055−7063.
(12) Zhu, A.; Zhao, Q. D.; Li, X. Y.; Shi, Y. $BiFeO_3/TiO_2$ Nanotube Arrays Composite Electrode: Construction, Characterization, and Enhanced Photoelectrochemical Properties. *ACS Appl. Mater. Interfaces* **2013**, *6*, 671−679.
(13) Beranek, R.; Macak, J. M.; Gärtner, M.; Meyer, K.; Schmuki, P. Enhanced Visible Light Photocurrent Generation at Surface-Modified TiO_2 Nanotubes. *Electrochim. Acta* **2009**, *54*, 2640−2646.
(14) Zhai, C. Y.; Zhu, M. S.; Lu, Y. T.; Ren, F. F.; Wang, C. Q.; Du, Y. K.; Yang, P. Reduced Graphene Oxide Modified Highly Ordered TiO_2 Nanotube Arrays Photoelectrode with Enhanced Photoelectrocatalytic Performance under Visible-Light Irradiation. *Phys. Chem. Chem. Phys.* **2014**, *16*, 14800−14807.
(15) Hou, Y.; Li, X. Y.; Zhao, Q. D.; Quan, X.; Chen, G. H. Electrochemical Method for Synthesis of a $ZnFe_2O_4/TiO_2$ Composite Nanotube Array Modified Electrode with Enhanced Photoelectrochemical Activity. *Adv. Funct. Mater.* **2010**, *20*, 2165−2174.
(16) Kontos, A. I.; Likodimos, V.; Stergiopoulos, T.; Tsoukleris, D. S.; Falaras, P.; Rabias, I.; Papavassiliou, G.; Kim, D.; Kunze, J.; Schmuki, P. Self-Organized Anodic TiO_2 Nanotube Arrays Functionalized by Iron Oxide Nanoparticles. *Chem. Mater.* **2009**, *21*, 662−672.
(17) Yuan, S. J.; Mu, J. K.; Mao, R. Y.; Li, Y. G.; Zhang, Q. H.; Wang, H. Z. All-Nanoparticle Self Assembly ZnO/TiO_2 Heterojunction Thin Films with Remarkably Enhanced Photoelectrochemical Activity. *ACS Appl. Mater. Interfaces* **2014**, *6*, 5719−5725.
(18) Hoang, S.; Guo, S. W.; Hahn, N. T.; Bard, A. J.; Mullins, C. B. Visible Light Driven Photoelectrochemical Water Oxidation on Nitrogen-Modified TiO_2 Nanowires. *Nano Lett.* **2011**, *12*, 26−32.
(19) Hwang, Y. J.; Hahn, C.; Liu, B.; Yang, P. D. Photoelectrochemical Properties of TiO_2 Nanowire Arrays: A Study of the Dependence on Length and Atomic Layer Deposition Coating. *ACS Nano* **2012**, *6*, 5060−5069.
(20) Song, P.; Zhang, X. Y.; Sun, M. X.; Cui, X. L.; Lin, Y. H. Graphene Oxide Modified TiO_2 Nanotube Arrays: Enhanced Visible Light Photoelectrochemical Properties. *Nanoscale* **2012**, *4*, 1800−1804.
(21) Xu, Z. C.; Yang, W. Y.; Li, Q.; Gao, S.; Shang, J. K. Passivated n−p Co-Doping of Niobium and Nitrogen into Self-Organized TiO_2 Nanotube Arrays for Enhanced Visible Light Photocatalytic Performance. *Appl. Catal., B* **2014**, *144*, 343−352.
(22) Zhang, M.; Yu, X. L.; Lu, D. D.; Yang, J. J. Facile synthesis and enhanced visible light photocatalytic activity of N and Zr co-doped TiO_2 nanostructures from nanotubular titanic acid precursors. *Nanoscale Res. Lett.* **2013**, *8*, 1−8.
(23) Zhang, M.; Wu, J.; Hou, J.; Yang, J. Molybdenum and Nitrogen Co-Doped Titanium Dioxide Nanotube Arrays with Enhanced Visible Light Photocatalytic Activity. *Sci. Adv. Mater.* **2013**, *5*, 535−541.
(24) Zhang, M.; Lu, D.; Zhang, Z.; Yang, J. Enhancement of Visible-Light-Induced Photocurrent and Photocatalytic Activity of V and N Codoped TiO_2 Nanotube Array Films. *J. Electrochem. Soc.* **2014**, *161*, H416−H421.
(25) Lu, D.; Zhang, M.; Zhang, Z.; Li, Q.; Wang, X.; Yang, J. Self-Organized Vanadium and Nitrogen Co-Doped Titania Nanotube Arrays with Enhanced Photocatalytic Reduction of CO_2 into CH_4. *Nanoscale Res. Lett.* **2014**, *9*, 272.
(26) Dai, G. P.; Yu, J. G.; Liu, G. Synthesis and Enhanced Visible-Light Photoelectrocatalytic Activity of p−n Junction $BiOI/TiO_2$ Nanotube Arrays. *J. Phys. Chem. C* **2011**, *115*, 7339−7346.
(27) Wu, Q.; Ouyang, J. J.; Xie, K. P.; Sun, L.; Wang, M. Y.; Lin, C. J. Ultrasound-Assisted Synthesis and Visible-Light-Driven Photocatalytic Activity of Fe-Incorporated TiO_2 Nanotube Array Photocatalysts. *J. Hazard. Mater.* **2012**, *199−200*, 410−417.
(28) Wang, M. Y.; Sun, L.; Lin, Z. Q.; Cai, J. H.; Xie, K. P.; Lin, C. J. p-n Heterojunction Photoelectrodes Composed of Cu_2O-Loaded TiO_2 Nanotube Arrays with Enhanced Photoelectrochemical and Photoelectrocatalytic Activities. *Energy Environ. Sci.* **2013**, *6*, 1211−1220.
(29) Liu, J. Q.; Ruan, L. L.; Adeloju, S. B.; Wu, Y. C. $BiOI/TiO_2$ Nanotube Arrays, a Unique Flake-Tube Structured p-n Junction with Remarkable Visible-Light Photoelectrocatalytic Performance and Stability. *Dalton Trans.* **2014**, *43*, 1706−1715.
(30) Tan, C. W.; Zhu, G. Q.; Hojamberdiev, M.; Okada, K.; Liang, J.; Luo, X. C.; Liu, P.; Liu, Y. Co_3O_4 Nanoparticles-Loaded BiOCl Nanoplates with the Dominant {001} Facets: Efficient Photodegradation of Organic Dyes under Visible Light. *Appl. Catal., B* **2014**, *152−153*, 425−436.
(31) Warang, T.; Patel, N.; Santini, A.; Bazzanella, N.; Kale, A.; Miotello, A. Pulsed Laser Deposition of Co_3O_4 Nanoparticles Assembled Coating: Role of Substrate Temperature to Tailor Disordered to Crystalline Phase and Related Photocatalytic Activity in Degradation of Methylene Blue. *Appl. Catal., A* **2012**, *423−424*, 21−27.
(32) Jiao, F.; Frei, H. Nanostructured Cobalt Oxide Clusters in Mesoporous Silica as Efficient Oxygen-Evolving Catalysts. *Angew. Chem., Int. Ed.* **2009**, *48*, 1841−1844.
(33) Xie, X. W.; Li, Y.; Liu, Z. Q.; Haruta, M.; Shen, W. J. Low-Temperature Oxidation of CO Catalysed by Co_3O_4 Nanorods. *Nature* **2009**, *458*, 746−749.
(34) Tyo, E. C.; Yin, C. R.; Di Vece, M.; Qian, Q.; Kwon, G.; Lee, S.; Lee, B.; DeBartolo, J. E.; Seifert, S.; Winans, R. E.; Si, R.; Ricks, B.; Goergen, S.; Rutter, M.; Zugic, B.; Flytzani-Stephanopoulos, M.; Wang, Z. W.; Palmer, R. E.; Neurock, M.; Vajda, S. Oxidative Dehydrogenation of Cyclohexane on Cobalt Oxide (Co_3O_4) Nanoparticles: The Effect of Particle Size on Activity and Selectivity. *ACS Catal.* **2012**, *2*, 2409−2423.
(35) Compton, O. C.; Abouimrane, A.; An, Z.; Palmeri, M. J.; Brinson, L. C.; Amine, K.; Nguyen, S. T. Exfoliation and Reassembly of Cobalt Oxide Nanosheets into a Reversible Lithium-Ion Battery Cathode. *Small* **2012**, *8*, 1110−1116.
(36) Liao, L. B.; Zhang, Q. H.; Su, Z. H.; Zhao, Z. Z.; Wang, Y. N.; Li, Y.; Lu, X. X.; Wei, D. G.; Feng, G. Y.; Yu, Q. K.; Cai, X. J.; Zhao, J. M.; Ren, Z. F.; Fang, H.; Robles-Hernandez, F.; Baldelli, S.; Bao, J. M. Efficient Solar Water-Splitting Using a Nanocrystalline CoO Photocatalyst. *Nat. Nanotechnol.* **2014**, *9*, 67−73.
(37) Wang, H. G.; Ma, D. L.; Huang, X. L.; Huang, Y.; Zhang, X. B. General and Controllable Synthesis Strategy of Metal Oxide/TiO_2 Hierarchical Heterostructures with Improved Lithium-Ion Battery Performance. *Sci. Rep.* **2012**, *2*, 701.
(38) Wang, Y. F.; Hsieh, M. C.; Lee, J. F.; Yang, C. M. Nonaqueous Synthesis of CoO_x/TiO_2 Nanocomposites Showing High Photocatalytic Activity of Hydrogen Generation. *Appl. Catal., B* **2013**, *142−143*, 626−632.
(39) Cao, C. L.; Hu, C. G.; Shen, W. D.; Wang, S. X.; Wang, J. L.; Tian, Y. S. Fabrication of a Novel Heterostructure of Co_3O_4-Modified TiO_2 Nanorod Arrays and Its Enhanced Photoelectrochemical Property. *J. Alloys Compd.* **2013**, *550*, 137−143.
(40) Zhang, G. G.; Huang, H. T.; Li, W. F.; Yu, F.; Wu, H. J.; Zhou, L. M. Enhanced Photocatalytic Activity of CoO/TiO_2 Nanotube Composite. *Electrochim. Acta* **2012**, *81*, 117−122.
(41) Luo, J. S.; Karuturi, S. K.; Liu, L. J.; Su, L. T.; Tok, A. I. Y.; Fan, H. J. Homogeneous Photosensitization of Complex TiO_2 Nanostructures for Efficient Solar Energy Conversion. *Sci. Rep.* **2012**, *2*, 451.
(42) Riha, S. C.; Klahr, B. M.; Tyo, E. C.; Seifert, S.; Vajda, S.; Pellin, M. J.; Hamann, T. W.; Martinson, A. B. F. Atomic Layer Deposition of a Submonolayer Catalyst for the Enhanced Photoelectrochemical Performance of Water Oxidation with Hematite. *ACS Nano* **2013**, *7*, 2396−2405.
(43) Lichterman, M. F.; Shaner, M. R.; Handler, S. G.; Brunschwig, B. S.; Gray, H. B.; Lewis, N. S.; Spurgeon, J. M. Enhanced Stability and Activity for Water Oxidation in Alkaline Media with Bismuth Vanadate Photoelectrodes Modified with a Cobalt Oxide Catalytic Layer Produced by Atomic Layer Deposition. *J. Phys. Chem. Lett.* **2013**, *4*, 4188−4191.
(44) Biesinger, M. C.; Payne, B. P.; Grosvenor, A. P.; Lau, L. W. M.; Gerson, A. R.; Smart, R. S. C. Resolving Surface Chemical States in

XPS Analysis of First Row Transition Metals, Oxides and Hydroxides: Cr, Mn, Fe, Co and Ni. *Appl. Surf. Sci.* **2011**, *257*, 2717−2730.
(45) Pasko, S.; Abrutis, A.; Hubert-Pfalzgraf, L. G.; Kubilius, V. Cobalt (II) β-Diketonate Adducts as New Precursors for the Growth of Cobalt Oxide Films by Liquid Injection MOCVD. *J. Cryst. Growth* **2004**, *262*, 653−657.
(46) Barreca, D.; Massignan, C.; Daolio, S.; Fabrizio, M.; Piccirillo, C.; Armelao, L.; Tondello, E. Composition and Microstructure of Cobalt Oxide Thin Films Obtained from a Novel Cobalt(II) Precursor by Chemical Vapor Deposition. *Chem. Mater.* **2001**, *13*, 588−593.
(47) Shahed, U. M. K.; Mofareh, A. S.; William, B. I., Jr. Biofunctional TiO_2 Nanoparticle-Mediated Photokilling of Cancer Cells Using UV Irradiation. *Science* **2002**, *297*, 2243−2245.
(48) Yamamoto, H.; Tanaka, S.; Hirao, K. Effects of Substrate Temperature on Nanostructure and Band Structure of Sputtered Co_3O_4 Thin Films. *J. Appl. Phys.* **2003**, *93*, 4158−4162.
(49) Sivula, K.; Zboril, R.; Le Formal, F.; Robert, R.; Weidenkaff, A.; Tucek, J.; Frydrych, J.; Grätzel, M. Photoelectrochemical Water Splitting with Mesoporous Hematite Prepared by a Solution-Based Colloidal Approach. *J. Am. Chem. Soc.* **2010**, *132*, 7436−7444.
(50) Jiao, Z. B.; Chen, T.; Xiong, J. Y.; Wang, T.; Lu, G. X.; Ye, J. H.; Bi, Y. P. Visible-Light-Driven Photoelectrochemical and Photocatalytic Performances of Cr-Doped $SrTiO_3/TiO_2$ Heterostructured Nanotube Arrays. *Sci. Rep.* **2013**, *3*, 2720.
(51) Edge, L. F.; Schlom, D. G.; Chambers, S. A.; Cicerrella, E.; Freeouf, J. L.; Holländer, B.; Schubert, J. Measurement of the band offsets between amorphous $LaAlO_3$ and silicon. *Appl. Phys. Lett.* **2004**, *84*, 726−728.